Achievable Rate Optimization of the RIS-Aided Near-Field Wideband Uplink

Yajun Cheng, Chongwen Huang, *Member, IEEE*, Wei Peng, *Senior Member, IEEE*, Mérouane Debbah, *Fellow, IEEE*, Lajos Hanzo, *Fellow, IEEE*, and Chau Yuen, *Fellow, IEEE*

***Abstract*—In this work, we investigate the performance of reconfigurable intelligent surface (RIS) assisted near-field wideband system. By considering the large-scale effect of a high-dimensional RIS and frequency-selective channels, we derive an accurate array manifold of the RIS in the near-field from the scattering point of view. Subsequently, we conceive a near-optimal RIS phase design for a single-user scenario to alleviate the beam-squint effect of the wideband system. As for the multi-user case, we provide a virtual-subarray-based phase shift design, which mitigates the beam-squint effect as well as the mitigates deleterious effects of beam concentration. Numerical results show that the achievable data rate can be significantly improved by the proposed schemes compared to the benchmarks both in the single-user and multi-user cases. Explicitly, in the multi-user system, by leveraging the virtual-subarray-based phase design, the achievable sum-rate can be doubled compared to the conventional benchmarks.**

***Index Terms*—Reconfigurable intelligent surface, near-field, wideband communications, beam squint, rate optimization, phase design**

The work of was supported in part by the National key research and development program under Grant 2019YFE0110200, the National Natural Science Foundation of China under Grants 62171192, U20B2060 and the Innovative Project of Shenzhen city in China under Grant JCYJ20210324135206018. The work of Chongwen Huang was supported by was supported by the China National Key R&D Program under Grant 2021YFA1000500, National Natural Science Foundation of China under Grant 62101492, Zhejiang Provincial Natural Science Foundation of China under Grant LR22F010002, Zhejiang University Global Partnership Fund, Zhejiang University Education Foundation Qizhen Scholar Foundation, and Fundamental Research Funds for the Central Universities under Grant 2021FZZX001-21. The work of Lajos Hanzo was supported by the Engineering and Physical Sciences Research Council projects EP/W016605/1, EP/X01228X/1 and EP/X01228X/1 as well as of the European Research Council's Advanced Fellow Grant QuantCom (Grant No. 789028). The work of Chau Yuen was supported by the Ministry of Education, Singapore, under its MOE Tier 2 (Award number MOE-T2EP50220-0019). Any opinions, findings and conclusions or recommendations expressed in this material are those of the author(s) and do not reflect the views of the Ministry of Education, Singapore.

Yajun Cheng is with the School of Cyber Science and Engineering, the School of Electronic Information and Communications, Huazhong University of Science and Technology, and also with the State Key Laboratory of Integrated Service Networks, Xidian University, Xian 710071, China. Part of this work was done by Yajun Cheng during his visiting at Nanyang Technological University and Singapore University of Technology and Design, Singapore (e-mail: yajuncheng@hust.edu.cn).

Wei Peng is with the School of Cyber Science and Engineering, Huazhong University of Science and Technology, and with the Research Center of 6G Mobile Communications, Huazhong University of Science and Technology, 1037 Luoyu Road, Wuhan, 430074, China. (e-mail: pengwei@hust.edu.cn).

Chongwen Huang is with College of Information Science and Electronic Engineering, Zhejiang University, Hangzhou 310027, China, and with International Joint Innovation Center, Zhejiang University, Haining 314400, China, and also with Zhejiang Provincial Key Laboratory of Info. Proc., Commun. & Netw. (IPCAN), Hangzhou 310027, China. (e-mail: chongwenhuang@zju.edu.cn).

Mérouane Debbah is with Khalifa University of Science and Technology, P O Box 127788, Abu Dhabi, UAE, (e-mail: merouane.debbah@tii.ae).

Lajos Hanzo is with the School of Electronics and Computer Science, University of Southampton, Southampton, SO17 1BJ, U.K. (e-mail: lh@ecs.soton.ac.uk).

Chau Yuen is with the School of Electrical and Electronics Engineering Nanyang Technological University, Singapore 639798. (e-mail: chau.yuen@ntu.edu.sg).

The corresponding author of this work is Wei Peng.

I. Introduction

RECONFIGURABLE intelligent surfaces (RISs) constitute as one of the most promising next-generation solutions [1]. They are capable of beneficially manipulating the electromagnetic signals at a low cost with the aid of a large number of reflecting elements [2], [3].

In the RIS-aided wireless communication systems, in addition to the beamformer design at the transmitter or receiver, one of the most critical problems is the phase shift adjustment of each passive element according to the propagation environment encountered. This formulation leads to joint optimization of the beamformer weights and RIS phases. For instance, [4] and [5] studied the joint transmit precoding design of RIS-aided millimeter wave (mmWave) communications where [4] presented a gradient-projection based method for minimizing the mean-squared error between the received and transmitted symbols, while [5] analyzed the phase design of multi-RIS scenarios for maximizing the received signal power. Additionally, the authors of [6] proposed a cross-entropy based method for tackling this joint optimization problem in maximizing the sum-rate in Terahertz (THz) communications. By contrast, Wu *et al.* maximized the energy-efficiency of a THz system via matrix adaptation strategy [7]. As a further development, a deep reinforcement learning framework was designed in [8] for THz communications in case of unquantized phase shifts. Ning *et al.* reported on hierarchical codebooks constructed via beam training and proposed hybrid beamforming digital/analog schemes for RIS-aided multi-user THz communications [9]. Moreover, the authors of [10] and [11] presented discrete phase designs from a practical point of view, because it is impossible to achieve a perfect continuous-valued phase shift in practice due to hardware limitations.

Another key issue of RIS-aided communication systems is the characterization of the path loss relying on the channel modeling. In this content, E. Björnson and L. Sanguinetti investigated the power scaling laws for asymptotically large RISs and compared the performances of RIS-aided systems to those of traditional MIMO systems [12]. Danufane *et al.* in [13] introduced a path loss model for RIS-aided communication links by exploiting Green's theorem. Özdogan *et al.* in

[14] studied the path loss of RIS-aided systems based on the assumption that the incident signals are transversal polarized electromagnetic waves. Najafi *et al.* developed a RIS-aided channel model relying on arbitrary linearly polarized incident signals [15]. The authors in [16] presented a practical model by considering the radiative characteristics of RIS, in which the RIS unit is assumed as a non-isotropic radiator. Moreover, Tang *et al.* reported on the free-space path loss models of RIS-aided systems and confirmed these by experimental results [17].

Although some of the existing studies oriented towards RIS-aided wideband communications [4]–[8], their analyses and discussions are usually based on adopting a narrowband hypothesis where the channel models are assumed to be non-dispersive, and the phase optimization is carried out at the central carrier frequency. However, in wideband communications, the channels exhibit frequency-selectivity. For example, the bandwidth of mmWave carries may be as high as several Gigahertz (GHz), while that in THz communications ranges from 2.16 GHz to 69 GHz [18]. The beam-squint effect [19]–[22] caused by frequency-selective channels is one of the impediments hindering the development of wideband communications, which has been exploited in traditional wireless communication systems operating without RIS. For instance, the authors of [21] proposed a sparse phase shifter-based hybrid precoding architecture of which each antenna is controlled by a pair of phase shifters. The authors of [22] introduced a delay-phase precoding technology designed for hybrid beamforming, which involves time-delaying components. These works exploiting beam-split mitigation mostly rely on the hardware components, such as a phase shifter controller and time delaying components. Since the passive characteristics of RISs is their advantages, the undesired additional hardware components increase not only the complexity of the system, but also increase it's power consumption, resulting in low energy efficiency. Hence, the existing methods in the literature, where beam squint is mitigated/exploited without RIS, are not applicable to the RIS-aided wireless communication systems.

There is a paucity of literature on the beam-squint effect in RIS-aided wideband communications. To the best of our knowledge, the conference paper of Chen *et al.* [23] took the beam-squint effect into account on the achievable downlink rate of a RIS-aided MISO mmWave system. Their simulation results show that the performance degradation caused by the beam squint in a mmWave system exceeds 3 bit/s/Hz. This loss is aggravated upon increasing the bandwidth. This knowledge gap inspires us to investigate RIS-aided wideband MIMO systems and multi-user scenarios. Additionally, this phenomenon has also been noted by Hao *et al.* [24]. Additionally, this phenomenon has also been noted by Hao *et al.* [24]. However, only single-user scenario has been addressed and time delay-based method is only applicable to a specific type of RIS which utilizes delay-adjustable metasurfaces.

Moreover, severe propagation losses occur in mmWave or THz communications, hence resulting in short transmission distances [25]. In this context, the concepts of holographic communications [26], extremely large arrays [27], [28] and near-field communications [29] have attracted substantial attention, especially in RIS-aided scenarios where the transmitter or receiver, or even both, operate in the near-field region of the RIS. Hence, the traditional far-field assumptions are no longer applicable for the channel modeling and performance optimization of the near-field communications. For example, Decarli and Dardari in [30] modified the calculation of the near/far field boundary of a large-scale array from $2D^2/2\lambda$ [31] to $2D^2\cos^2\vartheta/2\lambda$ where ϑ is the angle with respect to the boresight direction, which is more accurate. Furthermore, they discussed the communication modes of the RIS-aided system in the near-field. Cui and Dai in [32] investigated the near-field channel estimation algorithms of RIS-aided communications, and analyzed the differences between the near-field and far-field channels in the angle-domain. Dovelos *et al.* in [33] studied the near-field response of holographic RIS-aided THz communications, and their results indicated that the traditional far-field manifold of the RIS is unsuitable, because the planar wavefront assumption is inaccurate in the near-field.

Against the above background, we investigate the achievable uplink (UL) rate of a RIS-aided near-field wideband system. The differences between the considered system and traditional RIS-aided system lie in the following aspects. Firstly, the RIS is deployed at the users' side, i.e., the users are close to the RIS. Thus, the traditional plane wavefront hypothesis is no longer applicable. Secondly, the path loss based on the far-field model, which ignores the effective area change of the RIS caused by the angle between the users and RIS, is no longer valid due to the near-field effect. Thirdly, the beam-squint effect engendered by the wide bandwidth will impact the performance. Fourthly, the RIS usually consists of large number of elements, forming a large-scale array where the signal delay experienced across the entire array cannot be neglected. Last but not least, it is quite difficult in practice to design or manufacture a RIS that can operate across a broad frequency range. Therefore, the design of the RIS phase shift and its performance optimization face new challenges in wideband systems.

To tackle the above issues, we firstly analyze the behavior of the RIS in the near-field and characterize the path loss of RIS-aided near-field communications. Subsequently, we deduce the RIS-aided channel model of near-field communications after investigating both the large-scale and the beam-squint effects. Then, we reformulate the achievable UL rate and provide phase design schemes. Particularly, we propose a phase shift design based on a virtual subarray strategy. In this way, we can design the phase shift of the subarray according to the corresponding center frequency of each subcarrier instead of the center frequency of the wideband system. Therefore, the complexity of hardware implementation will be greatly reduced. In a nutshell, the main contributions of this paper are as follows:

- **Accurate array manifold of the RIS in near-field wideband communications:** We analyze the path loss of the RIS from the scattering point of view and deduce an accurate array manifold, i.e., array response vector of the RIS by explicitly taking both the large-scale and beam-squint effects into account.
- **Frequency-dependent phase shift (FDPS) design in**

single-user scenario: We investigate both the optimal and near-optimal phase shifts of the RIS in orthogonal frequency division multiplexing (OFDM) systems, and conceive a phase design based on non-uniform frequency response in a single-user scenario for mitigating the rate erosion caused by beam squint.

- **Virtual-subarray-based (VSA-based) phase shift design in multi-user scenario:** We provide a phase shift design based on the virtual subarray method capable of forming multiple beams in multi-user scenario, which mitigates the beam-squint effect as well as avoids the beam concentration problem.
- **Performance characterization of the proposed algorithms:** We present numerical results characterizing the proposed FDPS and VSA-based schemes, and compare them to the traditional phase shift that is designed according to the central carrier frequency. The results confirm that the proposed methods effectively mitigate the beam-squint effects, thereby improving the achievable UL sum-rate.

The remainder of this paper is organized as follows. We present the system model and describe the optimization objective in Section II. The reflection model of the RIS elements and RIS-based path loss are introduced in Section III, along with the large-scale and beam-squint effects involved. Then, in Section IV, our near-optimal solution and phase design algorithms are proposed for the considered system. Finally, we provide our simulation results and conclusions in Sections V and VI, respectively.

Notation: The boldface letters in lower and upper cases denote vectors and matrices, respectively; $\mathbb{C}^{M\times N}$ represents the space of an $M \times N$ complex-valued matrix; $(\cdot)^T$ and $(\cdot)^*$ denote the transpose and conjugate transpose operations, respectively; $\lfloor\cdot\rfloor$ is the floor operation; the $\mod(x, y)$ operator returns the remainder of x/y and $\mathrm{sort}(\cdot)$ represents the operation of sorting in ascending order; $|\cdot|$ and $\|\cdot\|$ represent the modulus operator and the Euclidean norm, respectively. Please note that due to different implementation processes or materials, different types of RIS may have different functions, such as reflection, transmission/refraction, polarization and even absorption [2], [34]. However, we only discuss the performance of RISs operating in the reflective mode.

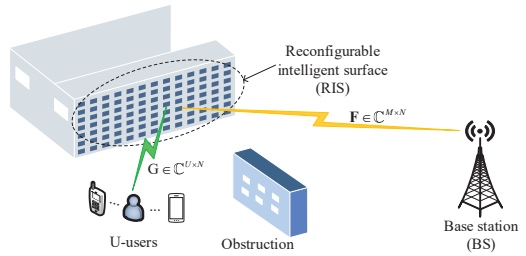

Fig. 1. System model.

II. System Description and Problem Formulation

By optimizing the phase shift, we maximize the achievable rates of RIS-aided wireless communication systems where the RIS is employed at the users' side for the following reasons. According to prior research in [34], the RIS should be preferably located close to the transmitter or receiver due to the "product path-loss" observation. Additionally, near-field wireless communications have attracted increasing interest [29]. Finally, most of the existing literature is dedicated to scenarios where the RIS is close to the base station (BS) [27], [35], [36], but there is a paucity of literature on the scenarios of having the RIS close to the users.

As illustrated in Fig. 1, there are U users in the vicinity of the RIS having N reflecting elements that is attached to the facade of buildings. Without loss of generality, a single-antenna is assumed at each user, while the BS antenna has M elements. The direct links between the BS and users are assumed to be blocked and hence they are neglected. Leveraging OFDM technique, the wide operational bandwidth is divided into numerous non-dispersive parallel sub-channels, i.e., the dispersion is completely eliminated. Hence in this manuscript, we investigate the optimization of a wideband OFDM system.

We assume that there are K subcarrires in the bandwidth of B having the center frequency f_c. Hence, the center frequency of subcarrier k^{th} is $f_k = f_c + \frac{B}{K}\left(k - \frac{K+1}{2}\right)$. Let $\mathbf{G}_k = [\mathbf{g}_{1,k}, \ldots, \mathbf{g}_{U,k}] \in \mathbb{C}^{N\times U}$ represents the channel matrix between the U users and the RIS, and $\mathbf{F}_k \in \mathbb{C}^{M\times N}$ be the channel matrix between the RIS and the BS over the k^{th} subcarrier, respectively, where $\mathbf{g}_{u,k}$ denotes the channel between the u^{th} user and the RIS over k^{th} subcarrier. Hence, the equivalent UL channel via the RIS is $\mathbf{H}_k = \mathbf{F}_k\mathbf{\Theta}\mathbf{G}_k$, where $\mathbf{\Theta} \in \mathbb{C}^{N\times N}$ is a diagonal matrix having the n^{th} elements of $\Theta_n = A_n e^{j\psi_n}$, which represents the reflecting coefficients with A_n and ψ_n representing the reflected amplitude and phase shift, respectively.

In the UL transmission, taking the k^{th} subcarrier as an example, the signal received at the BS over the k^{th} subcarrier is given by

$$\mathbf{r}_k = \sqrt{p}\mathbf{W}^*\mathbf{H}_k\mathbf{x} + \mathbf{n}, \tag{1}$$

where p is the average transmit power of each user and $\mathbf{W} \in \mathbb{C}^{M\times U}$ denotes the beamforming vector at the BS. $\mathbf{x} \in \mathbb{C}^{U\times 1}$ is the vector of transmitted symbols from the users. $\mathbf{n} \in \mathbb{C}^{M\times 1}$ denotes the vector of additive white Gaussian noises with each element having a zero mean and a variance σ^2.

Furthermore, we define $r_{u,k}$ and x_u as the u^{th} entry of $\mathbf{r}_k$ and $\mathbf{x}$, respectively. Additionally, $\mathbf{w}_{u,k}$ and $\mathbf{h}_{u,k} = \mathbf{F}\mathbf{\Theta}\mathbf{g}_{u,k}$ are the u^{th} columns of $\mathbf{W}_k$ and $\mathbf{H}_k$, respectively. Hence, the signal received at the BS from the u^{th} user over the k^{th} subcarrier is given by

$$r_{u,k} = \sqrt{p}\mathbf{w}_{u,k}^*\mathbf{h}_{u,k}x_u + \sqrt{p}\sum_{i=1,i\neq u}^{U}\mathbf{w}_{u,k}^*\mathbf{h}_{i,k}x_i + \mathbf{w}_{u,k}^*n. \tag{2}$$

Our objective is to maximize the achievable sum-rate at the BS, which is formulated as where $R_{u,k}$ is the achievable UL rate of the u^{th} user over the k^{th} subcarrier.

Similar problems concerning joint beamforming and phase optimization have been studied in the context of narrow-band systems in [4]–[9]. But this problem presents new challenges

$$\mathcal{P}0: \quad R=\max_{\mathbf{W},\boldsymbol{\Theta}} \frac{1}{K}\sum_{u=1}^{U}\sum_{k=1}^{K}\underbrace{\log_2\left(1+\frac{p\left|\mathbf{w}_{u,k}^{*}\mathbf{h}_{u,k}\right|^2}{p\sum_{i=1,i\neq u}^{U}\left|\mathbf{w}_{u,k}^{*}\mathbf{h}_{i,k}\right|^2+\|\mathbf{w}_{u,k}\|^2\sigma^2}\right)}_{R_{u,k}} \tag{3}$$
$$s.t.\ C_1:\|\mathbf{w}_u\|=1, u\in[1,\ldots,U],$$
$$C_2:|[\boldsymbol{\Theta}]_n|=1, n\in[1,\ldots,N],$$

in near-field communications, especially in wideband systems. On one hand, in near-field scenarios with the users close to the RIS, the path loss and array manifold based on the traditional far-field model become inaccurate, especially in the case of large scale RISs. On the other hand, the phase shift design based on the conventional narrowband assumption results in performance loss in wideband systems, since it neglects the beam squint caused by the wide bandwidth. Finally, the beam concentration problem where the beam may be focused on a fraction of the users population, or even on an individual, results in poor performance for the remaining users and has a grace impact on the total performance in multi-user systems.

To circumvent these issues, an accurate channel model is conceived for RIS-aided near-field wideband systems and we find a solution for problem $\mathcal{P}0$ in this new context.

III. RIS-AIDED PATH-LOSS AND ARRAY MANIFOLD

To the best of our knowledge, the path loss based on the far-field channel model is inaccurate in the near-field scenario, and the time delay across a large RIS arrays becomes non-negligible, especially in wideband systems [30]–[33]. Additionally, the inherent beam squint [19], [20], [23] caused by the wide bandwidth degrades the performance quite significantly, as detailed below.

A. RIS-aided path loss

Fig. 2 depicts the scattering model of a single RIS element where the incident wave is a parallel polarized uniform plane wave. The size of the RIS element is $a\times b$, and d_i represents the distance travelled by the incident signal from the transmitter to the RIS. Additionally, θ_i refers to the angle of the incident signal from the z axis.

Based on electromagnetic theory [31], [33], the incident electric and magnetic fields are given by

$$\mathbf{E}^i=\sqrt{\frac{Z_0G_tP_t}{2\pi d_i^2}}\left(\mathbf{e}_y\cos\theta_i+\mathbf{e}_z\sin\theta_i\right)e^{-jw\left(y'\sin\theta_i-z'\cos\theta_i\right)}, \tag{4}$$

$$\mathbf{M}^i=\sqrt{\frac{G_tP_t}{2Z_0\pi d_i^2}}\mathbf{e}_x e^{-jw\left(y'\sin\theta_i-z'\cos\theta_i\right)}, \tag{5}$$

where G_t and P_t denote the antenna gain and transmit power, respectively. Additionally, Z_0 denotes the characteristic impedance of the medium. Moreover, $\mathbf{e}_x$, $\mathbf{e}_y$ and $\mathbf{e}_z$ are the unit vectors, while $w=2\pi/\lambda$ denotes the wave number.

Building on the analyses in [31, Example 6-5], the components of scattered electric field at the point with the distance

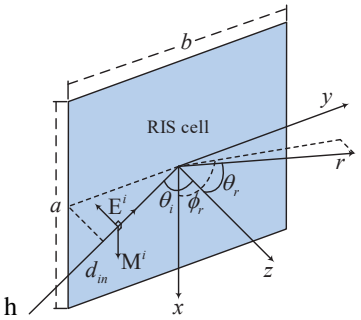

Fig. 2. Reflecting model of a single RIS element.

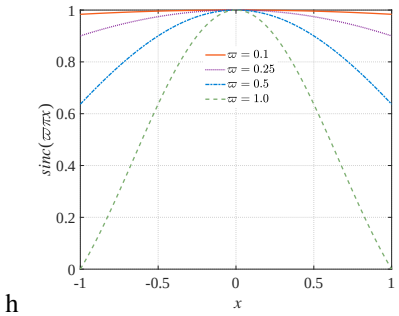

Fig. 3. $sinc(\varpi\pi x)$ v.s. x.

d_r and angle (θ,ϕ) are respectively given by

$$E_\theta\simeq -j\sqrt{\frac{Z_0G_tP_t}{2\pi d_i^2}}\frac{a\cdot b\cdot ke^{-jwd_r}}{2\pi d_r}\cos\theta\cdot\sin\phi\cdot sincX\cdot sincY, \tag{6}$$

$$E_\phi\simeq -j\sqrt{\frac{Z_0G_tP_t}{2\pi d_i^2}}\frac{a\cdot b\cdot ke^{-jwd_r}}{2\pi d_r}\cos\phi\cdot sincX\cdot sincY, \tag{7}$$

where $sincx=\sin x/x$, $X=a\cdot w\cdot\sin\theta\cdot\cos\phi/2$, and $Y=b\cdot w\cdot(\sin\theta\cdot\sin\phi-\sin\theta_i)/2$.

Thus, assuming a receiver having an ommi-directional single-antenna whose effective area is $A_r=\lambda^2G_r/(4\pi)$, the corresponding power at this point is given

$$\begin{aligned}P_r&=\frac{E^2}{2Z_0}\\&\overset{(a)}{=}\frac{a^2b^2G_tP_t}{4\pi\lambda^2d_i^2d_r^2}sinc^2X\cdot sinc^2Y\left(\cos^2\theta\cdot\sin^2\phi+\cos^2\phi\right),\\&\overset{(b)}{=}\frac{a^2b^2G_tG_rP_t}{\left(4\pi d_id_r\right)^2}sinc^2X\cdot sinc^2Y\left(\cos^2\theta\cdot\sin^2\phi+\cos^2\phi\right)\end{aligned} \tag{8}$$

where (a) and (b) follow upon substituting $E = \sqrt{(E_\theta)^2 + (E_\phi)^2}$ and A_r, successively. Please note that we analyze the characteristic of the RIS in its radiating near-field (Fresnel) region, but not in its reactive near-field region [33]. Hence, the "back-coupling" effects occurring in the reactive near-field of the nearby antennas/elements are neglected.

***Proposition** 1:* With the aid of the RIS, the path loss ρ between the source signal and receiver through a RIS element is given by

$$\rho = \frac{P_r}{P_t} = \underbrace{a \cdot b \cdot G_t / \left(4\pi d_i^2\right)}_{\rho(d_i)} \cdot \underbrace{a \cdot b \cdot G_r \cdot \cos^2\theta / \left(4\pi d_r^2\right)}_{\rho(d_r,\theta)}. \tag{9}$$

Proof: The derivation is omitted for simplicity, which is similar to that of [14, Lemma 2]. ■

This decoupled form in (9) can fortunately help us gain a better understanding of the RIS-aided path loss, which has two parts, the distance-dependent path loss as d_i and d_r, respectively. Additionally, $a \cdot b \cdot \cos^2\theta$ in $\rho(d_r, \theta)$ is related to the effective areas in the direction of θ, which are defined as the area that is exactly perpendicular to the direction of propagation [14]. A similar path loss model has been presented in [14, Eq. (20)], in which the last term $\cos\theta_i$ is approximated by 1, because the incident signals are assumed to be planar waves.

***Lemma** 1:* In RIS-aided wireless communications, if either the user or the BS having antenna gain G and distance d from the RIS is in the far-field of the RIS, the path loss between the user or BS and the RIS is calculated by $\rho(d) = a{\cdot}b{\cdot}G/\left(4\pi d^2\right)$. Conversely, when the user or BS is near the RIS, the path loss is $\rho(d,\theta) = a \cdot b \cdot G \cdot \cos^2\theta / \left(4\pi d^2\right)$.

B. Large-scale effect and beam squint

According to the Huygens-Fresnel wave propagation principle [37], the signals incident upon the RIS elements are slightly delayed versions of the original signal arriving from the users. Hence, take the u^{th} user as an example, assuming that the incident signal at the first element is $y_{1,u} = \alpha_{1,u} x_u(t)$, the baseband signal impinging at the n^{th} element from u^{th} user is given by

$$y_{n,u}(t) \triangleq \alpha_{n,u} x(t - \tau_{n,u}) e^{-j2\pi f_c \tau_{n,u}}, \tag{10}$$

where $\alpha_{n,u}$ and $\tau_{n,u} = (d_{n,u} - d_{1,u})/c$ denote the complex channel gain and the corresponding path delay between the u^{th} user and the n^{th} element [38]. Additionally, $d_{n,u}$ denotes the distance from the u^{th} user to the n^{th} RIS element, while c is the speed of light.

If the RIS is small, we have $x(t - \tau_m) \approx x(t)$. However, a high-dimensional RIS yields a non-negligible delay across the array. Hence, $(d_{n,u} - d_{1,u})/c$ can no longer be ignored. In the other words, the approximation $x(t - \tau_{n,u}) \approx x(t)$ no longer holds for a large RIS. For instance, for a uniform linear array equipped with 128 elements and half-wavelength element-spacing, when the incident path impinges from $\vartheta = 60°$, the propagation delays across the array aperture are $0.58T_s$ and $0.92T_s$ in a typical LTE system (transmission bandwidth 20 MHz, center frequency 1.9 GHz) and typical mmWave-band system (transmission bandwidth 1 GHz, center frequency 60 GHz), respectively, where T_s denotes the symbol period of the single-carrier signal [19]. For an increased RIS scale, this non-negligible delay across the array further aggravates. Hence, we refer to this phenomenon as the large-scale effect in this paper.

Naturally, the impulse response of the channel between the u^{th} user and n^{th} RIS element is

$$g_{n,u}(t) \triangleq \alpha_{n,u} \delta(t - \tau_{n,u}) e^{-j2\pi f_c \tau_{n,u}}, \tag{11}$$

where $\delta(\cdot)$ represents the Dirac impulse function. Upon taking the continuous-time Fourier transform of (11), we obtain the frequency-domain expression of

$$\begin{aligned} g_{n,u}(f) &= \alpha_{n,u} e^{-j\frac{2\pi f_c\left(d_{n,u} - d_{1,u}\right)}{c}} \int_{-\infty}^{\infty} \delta(t - \tau_{n,u}) e^{-j2\pi f t} dt \\ &= \alpha_{n,u} e^{-j\frac{4\pi f_c\left(d_{n,u} - d_{1,u}\right)}{c}} \end{aligned}. \tag{12}$$

Hence, the channel vector between the u^{th} user and the RIS can be written as

$$\mathbf{g}_u = \left[\alpha_{1,u}, \alpha_{2,u} e^{-j\frac{4\pi f_c\left(d_{2,u} - d_{1,u}\right)}{c}}, \ldots, \alpha_{N,u} e^{-j\frac{4\pi f_c\left(d_{N,u} - d_{1,u}\right)}{c}}\right]^T. \tag{13}$$

According to (9), $\alpha_{n,u} = \sqrt{a \cdot b \cdot G_u \cdot \cos^2\theta_{n,u} / \left(4\pi d_{n,u}^2\right)}$ with G_u representing the antenna gain of the u^{th} user. Additionally, $\theta_{n,u}$ denotes the angle from the u^{th} user to the n^{th} RIS element. Based on the geometrical structure, we have $d_{n,u} = \sqrt{d_{1,u}^2 + (n-1)^2 d_e^2 - 2(n-1) d_e d_{1,u} \sin\theta_{1,u}}$ and $d_{n,u}\cos\theta_{n,u} = d_{1,u}\cos\theta_{1,u}$.

Then, (13) can be rewritten as (14) at the bottom of this page where $\mathbf{b}(N, \mathbf{d}_u)$ denotes the *accurate manifold* of the RIS with $\mathbf{d}_u = [d_{1,u}, \ldots, d_{N,u}]$ representing the distance vector. Additionally, the corresponding traditional near-field array manifold of an array is [39, Eq. (20)]

$$\overline{\mathbf{b}}(N, \mathbf{d}) = \frac{1}{\sqrt{N}}\left[1, \frac{d_1}{d_2} e^{-j\frac{2\pi f_c(d_2 - d_1)}{c}}, \ldots, \frac{d_1}{d_N} e^{-j\frac{2\pi f_c(d_N - d_1)}{c}}\right]^T. \tag{15}$$

It is readily seen that compared to (15), the manifold in (14) is more accurate because it not only takes into account the delay of the spherical wavefront, but in reality the effective

$$\mathbf{g}_u = \sqrt{N}\alpha_{1,u} \underbrace{\frac{1}{\sqrt{N}}\left[1, \frac{d_{1,u}^2}{d_{2,u}^2} e^{-j\frac{4\pi f_c\left(d_{2,u} - d_{1,u}\right)}{c}}, \ldots, \frac{d_{1,u}^2}{d_{N,u}^2} e^{-j\frac{4\pi f_c\left(d_{N,u} - d_{1,u}\right)}{c}}\right]^T}_{\mathbf{b}(N, \mathbf{d}_u)}, \tag{14}$$

area also changes as a function of the incident/emission angle.

Furthermore, the propagation delay effects become more obvious for wideband systems, since the delay across the array becomes comparable to or even exceeds the symbol period [37]. Hence, the array manifold $\mathbf{b}\left(N,\mathbf{d}_u\right)$ in (14) is more accurate for wideband systems.

In the considered wideband OFDM system, the impulse response of the channel between the u^{th} user and n^{th} RIS element over the k^{th} subcarrier in (12) can be recast as

$$g_{n,u,k}\left(f_k\right)=\alpha_{n,u,k}e^{-j\frac{4\pi f_k\left(d_{n,u}-d_1\right)}{c}}, \tag{16}$$

where $f_k=f_c+\frac{B}{K}\left(k-\frac{K+1}{2}\right)$. Accordingly, in a wideband system, $\mathbf{b}\left(N,\mathbf{d}_u\right)$ can be recast as

$$\mathbf{b}\left(N,\mathbf{d}_u,f_k\right)=\frac{1}{\sqrt{N}}\left[1,\frac{d_{1,u}^2}{d_{2,u}^2}e^{-j\frac{4\pi f_k\left(d_{2,u}-d_{1,u}\right)}{c}},\ldots,\frac{d_{1,u}^2}{d_{N,u}^2}e^{-j\frac{4\pi f_k\left(d_{N,u}-d_{1,u}\right)}{c}}\right]^T. \tag{17}$$

As it can be observed, in wideband systems, the array manifold of the RIS is frequency-selective. Hence, the manifold of each subcarrier is different, which is known as the beam-squint effect in traditional massive antenna systems. Therefore, this manifold model will be adopted for our RIS-aided near-field wideband system hereafter.

The following proposition is presented to show that the phase shift mismatch will lead to a deterioration of the array gain and thus degrade the system performance. In addition, the corresponding simulation result will be shown in Section V-A.

***Proposition** 2:* Based on the array manifold in (17), we have $\left|\mathbf{b}^*\left(N,\mathbf{d},f_k\right)\mathbf{b}\left(N,\mathbf{d},f_i\right)\right|$ which may be approximated by

$$\begin{aligned}&\left|\mathbf{b}^*\left(N,\mathbf{d},f_k\right)\mathbf{b}\left(N,\mathbf{d},f_i\right)\right|\\&\leq\frac{1}{N\gamma\cos^3\theta_0}\left\{\frac{1}{2\cos\theta_0}\left[\arctan\left(\frac{4\gamma N\cos\theta_0}{4-N^2\gamma^2}\right)+c\pi\right],\right.\\&\left.+\frac{\gamma N\left(4\cos2\theta_0+N^2\gamma^2\right)}{2\left[\left(4+N^2\gamma^2\right)^2-\sin^2\theta_0N^2\gamma^2\right]}\right\}\end{aligned} \tag{18}$$

where we have $\gamma=d_e/d_0$, and d_0 denotes the distance from the transmitter or receiver to the RIS center. In addition, we have $c=0$, when $\gamma N<2\sin\theta_0$, otherwise, $c=1$.

Proof: Please see appendix A. ∎

When the BS or the user is far away from the RIS, far field assumption applies. With d_e being the element-spacing, we have $d_{N,u}-d_{1,u}=\left(N-1\right)d_e\sin\theta_{1,u}$, and the *approximate manifold* in the far-field is given by

$$\mathbf{a}\left(N,\theta_{1,u},f_k\right)=\frac{1}{\sqrt{N}}\left[1,e^{-j\frac{4\pi f_kd_e\sin\theta_{1,u}}{c}},\ldots,e^{-j\frac{4\pi f_k(N-1)d_e\sin\theta_{1,u}}{c}}\right]^T, \tag{19}$$

Please note that the element-spacing is based on the center frequency.

IV. Achievable rate analysis and phase shift optimization

In this section, we commence by analyzing the case of a single-user and proposing an algorithm for tackling the beam-squint effect to draw some useful insights. Then we expand our approach to a multi-user case. In the following discussions, perfect channel state information is assumed for simplicity to avoid detracting from phase-shift optimization, some channel estimation methods may be found in [40], [41]. Additionally, we assume that the theoretical phase shift of each RIS element can be perfectly matched with the actual phase shift. In other words, the phase shift is considered to be of infinite resolution. The discrete phase with finite resolution is beyond the scope of this paper and can be realized using existing methods [10], [11], [42].

A. Single-user scenario

In this subsection, we first discuss the case of one user. Again, we focus on user-side RIS where the user is in the near-field of the RIS. Hence, the plane wavefront assumption no longer holds, and the channel between the user and the RIS over the k^{th} subcarrier is

$$\mathbf{g}_k=\sqrt{N}\alpha_1\mathbf{b}\left(N,\mathbf{d},f_k\right), \tag{20}$$

where $\mathbf{b}\left(N,\mathbf{d},f_k\right)$ is the accurate manifold given in (17) and $\mathbf{d}=[d_1,\ldots,d_N]$. Additionally, $\alpha_1=\sqrt{a\cdot b\cdot G_u\cdot\cos^2\theta_1/\left(4\pi d_1^2\right)}$ is the path loss with θ_1 and d_1 denoting the angle and distance from the user to the 1^{st} RIS element, respectively.

As for the BS and RIS, we assume that they are in the far field of each other. Then, the channel between them over the k^{th} subcarrier is given by

$$\mathbf{F}_k=\sqrt{MN}\alpha_{RB}\mathbf{a}\left(M,\theta_{RB},f_k\right)\mathbf{a}^*\left(N,\varphi_{RB},f_k\right), \tag{21}$$

where $\alpha_{RB}=\sqrt{a\cdot b\cdot G_t/\left(4\pi d_{RB}^2\right)}$ with d_{RB} being the distance between the RIS and BS; θ_{RB} and φ_{RB} denote the angle of arrival and angle of departure from the RIS to BS, respectively.

Hence, in the single-user case, the problem $\mathcal{P}0$ of (3) is recast as

$$\begin{aligned}\mathcal{P}1:\quad&R_{\mathrm{SU}}=\max_{\mathbf{W},\boldsymbol{\Theta}}\ \frac{1}{K}\sum_{k=1}^{K}\log_2\left(1+\frac{p\left|\mathbf{w}_k^*\mathbf{h}_k\right|^2}{\sigma^2}\right),\\&s.t.\ \ C_1:\left\|\mathbf{w}_k\right\|=1,k\in[1,\ldots,K]\\&\qquad C_2:\left|\left[\boldsymbol{\Theta}\right]_n\right|=1,n\in[1,\ldots,N]\end{aligned} \tag{22}$$

where $\mathbf{h}_k=\mathbf{F}_k\boldsymbol{\Theta}\mathbf{g}_k$.

1) Near-optimal phase shift design of the RIS: It can be observed that the above problem cannot be solved directly, and the maximum rate can only be obtained by achieving the maximum rate over each subcarrier. Hence, we first discuss the phase design over the k^{th} subcarrier. The optimal phase shift achieving the maximum rate over the k^{th} subcarrier is

given by

$$\mathcal{P}2: \quad \overline{R}_k = \max_{\mathbf{W},\mathbf{\Theta}} \log_2\left(1+\frac{p\left|\mathbf{w}_k^*\mathbf{h}_k\right|^2}{\sigma^2}\right) \\ s.t.\ C_1: \|\mathbf{w}_k\| = 1, k \in [1,\ldots,K], C_2: \left|[\mathbf{\Theta}]_{n,k}\right| = 1 \tag{23}$$

According to [43], the maximum ratio combining (MRC) scheme is the optimal beamforming strategy at the BS in this case. Hence, to achieve the maximum rate over each subcarrier by the MRC scheme, we have the following insights.

***Theorem** 1:* In the single-user case, relying on the MRC strategy at the BS, the optimal phase shift of RIS maximizing the achievable rate over the k^{th} subcarrier is given by

$$\psi_{n,k}^{\text{opt}} = 4\pi\left[\frac{f_k\left(d_n-d_1\right)}{c} - \frac{f_k}{f_c}\epsilon_e(n-1)\sin\varphi_{RB}\right], \tag{24}$$

where $\epsilon_e = d_e/\lambda_c$ denotes the wave-length normalized spacing between adjacent RIS elements. The maximum achievable rate for this optimal phase shift is given by

$$\overline{R}_{\text{SU}} = \frac{1}{K}\sum_{k=1}^{K}\log_2\left(1+\frac{pMN\alpha_1^2\alpha_{RB}^2 d_1^2\sum_{n=1}^{N}\frac{A_n}{d_n^2}}{\sigma^2}\right). \tag{25}$$

Proof: Please see appendix B. ■

The optimal phase shift in (24) may indeed achieve the maximum rate over the k^{th} subcarrier, but it may reduce the rates of the other subcarriers due to the beam-squint. To be more concrete, with the phase shift $\psi_{n,k}^{\text{opt}}$ in (24), we can obtain the maximum of χ_k, but cannot get the maximum of χ_i when $i \neq k$. In other words, we can obtain the optimal rate $\overline{R}_k$ over the k^{th} subcarrier, but cannot guarantee the performance over the other subcarriers $f \neq f_k$. It should be noted that, although (25) can be used as an upper bound for the achievable rate in the single-user case, it is uneconomical to implement the solution in an actual wideband system. Therefore, it is necessary to investigate a compatible set of phase shifts for the whole band, which optimizes the achievable sum-rate of all the K subcarriers.

***Proposition** 3:* In the single-user case, relying on the MRC scheme at the BS, a near-optimal phase shift maximizing the achievable rate over the whole band is given by

$$\psi_n^{\text{near}} = 4\pi\left[\frac{f_c\left(d_n-d_1\right)}{c} - \epsilon_e\left(n-1\right)\sin\varphi_{RB}\right]. \tag{26}$$

Proof: Please see appendix C. ■

Although the phase shifts in (26) can achieve a near-optimal solution maximizing the rate across the whole band, they fail in alleviating the beam squint imposed by frequency-selectivity of the wideband systems, since they are based on f_c. To mitigate the beam-squint effects, we introduce a frequency-dependent phase shifting (FDPS) scheme in the following.

2) FDPS design of the RIS: According to the above discussions, the optimal phase shifts of (24) is frequency-dependent, while the near-optimal shift of (26) relies on the central carrier frequency f_c. However, neither of them can deal with the beam-squint effect. Based on these insights, we propose a FDPS design to reduce rate degradation caused by beam squint.

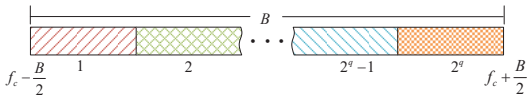

Fig. 4. Diagram of bandwidth division.

As illustrated in Fig. 4, the bandwidth B is evenly split into 2^q blocks. Hence, each block occupies the bandwidth of $B/2^q$, and the center frequency of each block is given by

$$f(t) = f_c - \frac{B}{2} + \frac{(2t-1)B}{2^{q+1}}, t \in [1,\ldots,2^q]. \tag{27}$$

Accordingly, the RIS is divided into 2^q subarrays virtually. Then, the number of elements in each subarray is given by

$$Num(t) = \begin{cases} \mathcal{N}_b, & t \in [1,\ldots,2^q-1] \\ N-(2^q-1)\mathcal{N}_b, & t = 2^q \end{cases}, \tag{28}$$

where we have $\mathcal{N}_b = \lfloor N/2^q \rfloor$ with $\lfloor\cdot\rfloor$ denoting the floor operation. Therefore, the index of each subarray element is given by

$$I(t) = \begin{cases} [(t-1)\mathcal{N}_b+1, t\mathcal{N}_b], & t \in [1,\ldots,2^q-1] \\ [(2^q-1)\mathcal{N}_b+1, N], & t = 2^q \end{cases}. \tag{29}$$

For notation simplicity, we define the frequency-dependent phase shift as $\psi[f(t)]$. According to (24) and (26), $\psi[f(t)]$ can be expressed as

$$\psi[f(t)] = 4\pi\left[\frac{f(t)\left(d_n-d_1\right)}{c} - \frac{f(t)}{f_c}\epsilon_e(n-1)\sin\varphi_{RB}\right]. \tag{30}$$

To avoid the phases concentrating on an individual frequency, we design the phases based on the above band division and virtual subarray methods. Specifically, the RIS is virtually divided into 2^q subarrays corresponding to 2^q band blocks. More concretely, for the t^{th} ($t \in [1, 2^q]$) subarray, the phase shift is designed according to $f(t)$ as expressed in (30).

The specific processes are presented in *Algorithm 1*. Please note that when the RIS is small, i.e., $\mathcal{N}_b < 1$ for a certain q, the phase can be designed based on the central carrier frequency f_c directly, or a smaller q should be used. The performance of this method will be evaluated via numerical simulations in Section V.

3) Complexity discussion in single-user scenario: According to the existing analyses, it is a consensus view that the complexity of MRC beamforming is proportional to the number of transmit antennas (N_t) and the number of receive antennas (N_r) in a massive input massive output system [45], [46]. Hence, we adopt $N_t \cdot N_r \cdot \mathcal{O}(MRC)$ to represent the complexity of the MRC scheme for a given N_t and N_r. The complexity of (24) is $M \cdot \mathcal{O}(MRC)$ and the complexity of the phase shift design associated with this scheme is $M \cdot N \cdot K \cdot \mathcal{O}(MRC)$. And the complexity of the phase shift design based on the phase shift in (26) is $M \cdot N \cdot \mathcal{O}(MRC)$, while the complexity of FDPS-based phase shift design is related to the parameter of q, and it is $M \cdot N \cdot 2^q \cdot \mathcal{O}(MRC)$.

Algorithm 1: The FDPS design in single-user scenario.

Input: Initial key parameters: M, N, a, b, p, f_c, K, B, G_t, G_u, d_{RB}, d_1, θ_1, q

Calculate $\mathcal{N}_b = \lfloor \frac{N}{2^q} \rfloor$;
if $\mathcal{N}_b \geq 1$ **then**
  Initialize $t = 1$;
  repeat
    foreach $n \in [(t-1)\mathcal{N}_b + 1, t\mathcal{N}_b]$ **do**
      $\psi_n^{\text{opt}} = \psi[f(t)]$ according to (30);
    $t = t + 1$;
  until $t > 2^q - 1$;
  foreach $n \in [(2^q - 1)\mathcal{N}_b + 1, N]$ **do**
    $\psi_n^{\text{opt}} = \psi[f(t)]$ according to (30);
else
  $\psi^{\text{opt}} = \psi(f_c)$ according to (30);

Output: The optimal phase shift of the RIS ψ^{opt}.

B. Multi-user scenario

In the previous section we have discussed the single user scenario where the phase shifts are designed from the perspective of maximizing the achievable rate over the whole band. However, this problem becomes more complex in the multiple users scenario where the sum-rate of all users to be considered. In other words, we need to maximize the achievable sum-rate, while additionally giving cognizance to the rate of each user.

We assume that there are U single-antenna users and each user transmits the signals at the power p. Analogous to the single-user case of (20), the channel between the u^{th} user and the RIS over the k^{th} subcarrier is given by

$$\mathbf{g}_{u,k} = \sqrt{N}\alpha_u \mathbf{b}(N, \mathbf{d}_u, f_k), \tag{31}$$

where $\alpha_u = \sqrt{G_u ab\cos^2\theta_{u,1}/\left(4\pi d_{u,1}^2\right)}$ is the path loss between the u^{th} and 1^{st} RIS element; $\theta_{u,1}$ and $d_{u,1}$ denote the angle and distance from the u^{th} user to the 1^{st} RIS element, respectively.

In this case, the problems $\mathcal{P}0$ and $\mathcal{P}1$ are rewritten as

$$\begin{aligned} \mathcal{P}3: \quad & R_{\text{MU}} = \max_{\mathbf{\Theta}} \frac{1}{K}\sum_{u=1}^{U}\sum_{k=1}^{K} R_{u,k} \\ & s.t.\ C_1: \mathbf{w}_{u,k} = \frac{\mathbf{h}_{u,k}}{\|\mathbf{h}_{u,k}\|}, C_2: \left|[\mathbf{\Theta}]_{n,u,k}\right| = 1 \end{aligned}. \tag{32}$$

1) Near-optimal phase shift design of the RIS: We firstly discuss the case of ideal phase shifts for each subcarrier, e.g. the k^{th} subcarrier. The achievable UL rate of the u^{th} user is

$$R_{u,k} = \log_2\left(1 + \frac{p\left|\mathbf{w}_{u,k}^* \mathbf{h}_{u,k}\right|^2}{p\sum_{i=1, i\neq u}^{U}\left|\mathbf{w}_{u,k}^* \mathbf{h}_{i,k}\right|^2 + \|\mathbf{w}_{u,k}\|^2 \sigma^2}\right). \tag{33}$$

Similarly to ***Theorem 1***, in the multi-user case, we have the following insight.

Theorem 2: For the sake of simplicity, we also adopt MRC-aided beamforming at the BS in the multi-user scenario considered, the optimal phase shift maximizing the achievable rate of the u^{th} user over the k^{th} subcarrier is given by

$$\psi_{n,u,k}^{\text{opt}} = 4\pi\left[\frac{f_k(d_{n,u} - d_{1,u})}{c} - \frac{f_k}{f_c}\epsilon_e(n-1)\sin\varphi_{RB}\right]. \tag{34}$$

The achievable rate R_{MU} in the multi-user scenario obeys

$$R_{\text{MU}} \leq \frac{1}{K}\sum_{k=1}^{K}\sum_{u=1}^{U}\log_2\left(1 + \frac{pMN\alpha_u^2\alpha_{RB}^2 d_{1,u}^2 \sum_{n=1}^{N}\frac{A_n}{d_{n,u}^2}}{\sigma^2}\right). \tag{35}$$

Proof: By substituting $\mathbf{w}_{u,k} = \mathbf{h}_{u,k}/\|\mathbf{h}_{u,k}\|$ into (33)and neglecting the interferences among the users, we have $R_{u,k} \leq \log_2(1 + p\|\mathbf{h}_{u,k}\|^2/\sigma^2)$. The proof is similar to that of ***Theorem 1***, hence omitted for simplicity. ■

Furthermore, analogous to ***Proposition 3***, the near-optimal phase design based on the central carrier frequency for the u^{th} user in this case is given by

$$\psi_{n,u}^{\text{near}} = 4\pi\left[\frac{f_c(d_{n,u} - d_{1,u})}{c} - \epsilon_e(n-1)\sin\varphi_{RB}\right]. \tag{36}$$

However, the above pair of phase shifts can neither guarantee the performance over the entire bandwidth nor can they alleviate the beam squint. Hence, we resort to a near-optimal problem by optimizing the upper-bound of the achievable sum-rate, and get the following near-optimal solution for the phase shifts.

Proposition 4: When employing MRC beamforming at the BS, a near-optimal phase shift maximizing the achievable multi-user sum-rate is given by

$$\widetilde{\psi}_n^{\text{near}} = \begin{cases} \frac{[\mathbf{T}_n]_{UK/2} + [\mathbf{T}_n]_{UK/2+1}}{2}, & \text{when} \mod(UK, 2) = 0 \\ [\mathbf{T}_n]_{(UK+1)/2}, & \text{when} \mod(UK, 2) = 1 \end{cases}, \tag{37}$$

where $\mathbf{T}_n = \text{sort}\big([J_{n,1,1}, \ldots, J_{n,1,K}, J_{n,2,1}, \ldots, J_{n,2,K}, \ldots, J_{n,U,1}, \ldots, J_{n,U,K}]\big)$, of which $J_{n,u,k} = 4\pi f_k[(d_{n,u} - d_{1,u})/c - \epsilon_e(n-1)\sin\varphi_{RB}/f_c]$.

Proof: Please see appendix D. ■

Based on the insights we gained, we have formulated the following properties.

Property 1: When we have $\mod(UK, 2) = 0$, we assume that the middle two terms of $\mathbf{T}_n$ are $J_{n,v,i}$ and $J_{n,u,k}$. Then, we have the following cases.

Case 1: When $v = u$ and $i \neq k$, the phase shift in (37) is based on the u^{th} user over the i^{th} and k^{th} subcarriers.

Case 2: When $v \neq u$ and $i = k$, the phase shift in (37) is based on two different users over an individual subcarrier, e.g. k^{th} subcarrier.

Case 3: When $v \neq u$ and $i \neq k$, the phase shift in (37) is based on two different users over two different subcarriers.

Property 2: When we have $\mod(UK, 2) = 1$, the optimal phase shift in (37) depends on an element of $\mathbf{T}_n$, which means that the phase shift is based on one user over one subcarrier.

In view of the above discussions, although the phase shifts in ***Proposition 4*** relieve the beam squint to some extent, it's benefit remains limited, because at most two subcarriers are involved in this method. Additionally, the phase shifts based on one or two users will impose the performance erosion on the remaining users. Hence, in the following, we propose a

phase shift design based on virtual subarray.

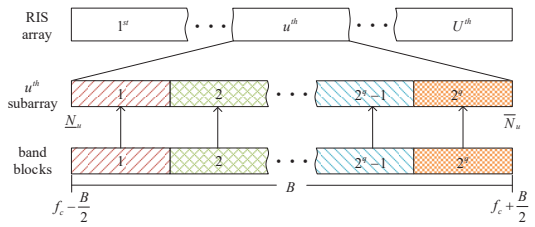

Fig. 5. Diagram of the phase shift design based on our VSA method.

2) VSA-based phase shift design of the RIS: As depicted in Fig. 5, the RIS array is divided into U subarrays virtually and the phase shift of each VSA specifically designed for the individual user. Please note that in this paper, we take RIS as a uniform linear array as an example for analysis. This method can be extended to a planar array, and each column or row of the planar array is divided in the same method. For instance, the phase shifts of the u^{th} subarray are designed for the u^{th} user leveraging the FDPS method as introduced in *Algorithm 1*. Additionally, $\underline{N}_u$ and $\overline{N}_u$ represent the first and last indexes of the u^{th} subarray. They are respectively given by

$$\underline{N}_u = (u-1)\,\mathcal{N}_a + 1,\ u \in [1,\ldots,U-1], \tag{38}$$

$$\overline{N}_u = \begin{cases} u\mathcal{N}_a,\ u \in [1,\ldots,U-1] \\ N,\ u = U \end{cases}, \tag{39}$$

where $\mathcal{N}_a = \lfloor N/2^q \rfloor$ denotes the number of elements in the subarray.

Additionally, according to the FDPS method, the index of each virtual subarray, such as the u^{th} subarray, is given by (40) at the bottom of this paper where $\mathcal{N}_u = \left\lfloor \left(\overline{N}_u - \underline{N}_u\right)/2^q \right\rfloor$ denotes the number of bands in the u^{th} subarray.

Analogous to (30), in this case, the phase shift of the u^{th} subarray with $f(t)$ is denoted by $\psi[u, f(t)]$ for ease of expression. According to (34) and (36), $\psi[u, f(t)]$ can be expressed as

$$\psi[u, f(t)] = 4\pi \left[\frac{f(t)\left(d_{n,u} - d_{1,u}\right)}{c} - \frac{f(t)}{f_c}\epsilon_e (n-1)\sin\varphi_{RB} \right]. \tag{41}$$

To illustrate this method intuitively, the processes are described in *Algorithm 2*.

3) Complexity discussion in multi-user scenario: According to the analysis of the complexity of (24), we can readily see that the complexity of the phase shift in (34) is $U{\cdot}M{\cdot}N{\cdot}K{\cdot}\mathcal{O}(MRC)$, while the complexity of the phase shift design based on the phase shift in (36) is $U{\cdot}M{\cdot}N{\cdot}\mathcal{O}(MRC)$. Finally, the complexity of the VSA-based phase design is $U \cdot M \cdot N \cdot 2^q \cdot \mathcal{O}(MRC)$.

Algorithm 2: The VSA-based phase design in multi-user scenario.

Input: Initial key parameters: M, N, a, b, p, f_c, K, B, G_t, G_u,d_{RB}, $d_{1,1},\ldots,d_{U,1}$, $\theta_{1,1},\ldots,\theta_{U,1}$, q

Calculate $\mathcal{N}_a = \left\lfloor \frac{N}{U} \right\rfloor$;
if $\mathcal{N}_a \geq 1$ **then**
  foreach $u \in [1, U-1]$ **do**
    $\underline{N}_u = (u-1)\,\mathcal{N}_a + 1, \overline{N}_u = u\mathcal{N}_a$;
  $\underline{N}_U = (U-1)\,\mathcal{N}_a + 1, \overline{N}_U = N$;
  foreach $u \in [1, U]$ **do**
    Calculate $\mathcal{N}_u = \left\lfloor \frac{\overline{N}_u - \underline{N}_u}{2^q} \right\rfloor$;
    if $\mathcal{N}_u \geq 1$ **then**
      Initialize $t = 1$;
      repeat
        foreach $n \in \left[\underline{N}_u + (t-1)\,\mathcal{N}_u + 1, \underline{N}_u + t\mathcal{N}_u\right]$ **do**
          $\psi_n^{\text{opt}} = \psi\left[u, f(t)\right]$;
        $t = t + 1$;
      until $t > 2^q - 1$;
      foreach $n \in \left[\underline{N}_u + (2^q-1)\,\mathcal{N}_u + 1, \overline{N}_u\right]$ **do**
        $\psi_n^{\text{opt}} = \psi\left[u, f(t)\right]$;
    else
      The phase shift is $\psi_n^{\text{opt}} = \psi(u, f_c)$;
else
  The phase shift is $\psi^{\text{opt}} = \psi(u, f_c)$;

Output: The optimal phase shift of the RIS ψ^{opt}.

V. Numerical Results

In this section, we characterize the performance of our RIS-aided near-field wideband system. As illustrated in Fig. 6, there are three users who are 5, 8, 10 meters away from the RIS center, respectively. The angles between the users and the RIS are independently and randomly distributed within $(0, 2\pi)$, and the results are based on the average of more than 1000 simulations. The central carrier frequency is $f_c = 300$ GHz, and the number of carriers is $K = 128$. The bandwidth B is varied from 5 GHz to 40 GHz. Additionally, the BS is assumed to be 10 meters away from the RIS with a uniform linear array of 64 antennas, i.e., $M = 64$. The number of the RIS elements N ranges from 48 to 1440, and the size of each RIS element is $0.1\lambda_c \times 0.1\lambda_c$ where $\lambda_c = c/f_c$. Moreover, the transmit power of each user is $p = 1$ mW, while the element-spacing of BS antennas and RIS are half the wave-length. Furthermore, the noise is calculated by $\sigma^2 = -174 + 10\lg B$. Please note that, unless otherwise indicated, we use $N = 1000$ and $B = 10$ GHz.

A. Array manifolds comparison

Firstly, as depicted in Fig. 7, we show the impact of the RIS manifold on the achievable rate. Two single-user scenarios are considered for comparison, namely the user distances of 5 and 50 meters. The performances marked by "Accurate"

$$I_u(t) = \begin{cases} \left[\underline{N}_u + (t-1)\,\mathcal{N}_u + 1, \underline{N}_u + t\mathcal{N}_u\right],\ t \in [1,\ldots,2^q-1] \\ \left[\underline{N}_u + (2^q-1)\,\mathcal{N}_u + 1, \overline{N}_u\right],\ t = 2^q \end{cases} \tag{40}$$

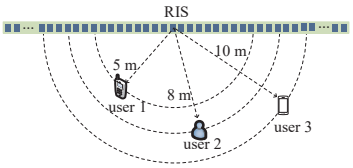

Fig. 6. Simulation scenario.

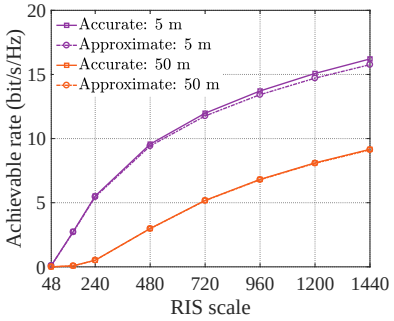

Fig. 7. Array manifold comparison.

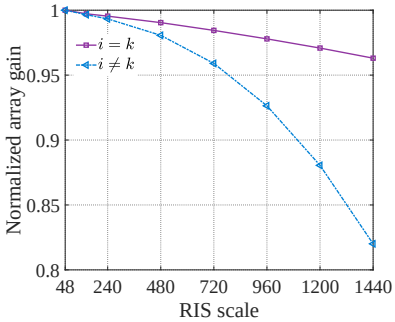

Fig. 8. Normalized array gain.

and "Approximate" are based on the array manifolds given in (17) and (19), respectively. As seen, for the distance of 50 meters, the rates are almost the same, since the two curves overlap. However, when the user is near the RIS, i.e., 5 meters, there exists a gap between the rates of the two manifolds, and their difference becomes more obvious with the increasing of RIS scale. Therefore, the manifold in (19) will be more accurate for the RIS-aided system, especially for near-field communication systems, and this one is adopted to describe the channel between the users and RIS hereafter.

Next, Fig. 8 presents the normalized array gain as discussed in (18) where k and i are randomly selected in $[1, \ldots, K]$, and $[1, \ldots, K]$ with $i \neq k$, respectively. Upon increasing RIS scale, the achievable rate exhibits a downward tendency. This decline is caused by the distance-dependent coefficient of each term of the array manifold in (19), which is always ignored in traditional systems. Additionally, for $i \neq k$, there is a performance loss, which becomes more serious upon increasing the scale of RIS. This phenomenon indicates the inherent bottleneck in the wideband system. Explicitly, when the phase shift is not matched to the operating frequency, a performance loss is unavoidable. Hence, it is necessary to conceive phase designs for mitigating the beam squint.

B. Achievable rate in single-user case

When presenting the simulation results, we use "Ideal" to represent the upper bound of the achievable rate in (25), where the phase shift is designed according to (24). The near-optimal phase design proposed in (26) is marked as "Prop: Near-opt". Additionally, the FDPS associated with different number of band blocks is marked as "Prop: $q = 1$", "Prop: $q = 2$", and "Prop: $q = 3$". Moreover, the scheme of [23] that is based on the central carrier frequency f_c is presented as a reference and marked as "Ref: Center-freq". Finally, in the single-user case, only the performance of user-1 is discussed as an example.

Fig. 9 showcases the achievable rate of different phase designs for a single user at different RIS scales, BWs, and SNRs where we have significant performance gaps between the "Ref: Central" and "Ideal" schemes. This shows that the central-frequency based phase shift, which is adopted in narrowband systems, is not applicable to wideband systems. These gaps indicate that the beam-squint effect caused by the wideband frequency-selective characteristics will impose substantial performance loss.

Fortunately, the proposed schemes are capable of reducing the performance penalty to some extent. To be quantitative, Fig. 9 (a) presents the achievable rate versus the RIS scale. It is clear that both the near-optimal scheme and the FDPS scheme outperform the central-frequency based scheme. As expected, the FDPS scheme is particularly beneficial for large scale RISs. More specifically, the FDPS scheme has the same performance improvements as the near-optimal scheme when the RIS is small, but outperforms the near-optimal scheme when the RIS scale is larger. Additionally, we observe that the maximum rates are obtained for $q = 1$, 2, and 3, when the RIS scale obeys $144 < N < 240$, $240 < N < 720$, and $N > 720$, respectively. This indicates that the parameter q also has a significant impact on the performance and a larger q should be adopted for a larger-scale RIS.

Furthermore, Fig. 9 (b) and Fig. 9 (c) illustrate the achievable rate for different BWs and SNRs, respectively. As observed, although adopting different q values has different effects on the achievable rate, the FDPS scheme outperforms the proposed near-optimal and the central-frequency based schemes by mitigating the beam squint. Moreover, the proposed near-optimal solution is superior to the central-frequency based scheme, because the latter ignores the large-scale effects of Section III-B.

C. Achievable sum-rate in multi-user scenario

Similar to the single-user case, the phase shift by (34) is marked as "Ideal" in the simulation results. The "Prop: Near-opt" scheme is the phase design of (37). The "Prop: $q = 1$", "Prop: $q = 2$" and "Prop: $q = 3$" accordingly denote the proposed VSA-based schemes corresponding to $q = 1$, 2, and 3, respectively. Finally, the "Ref: Center-freq" scheme of [23] is shown as a benchmark.

Fig. 10 depicts the achievable sum-rate of the three users seen in Fig. 6 at different RIS scales, BWs and SNRs. The proposed schemes, including near-optimal and VSA-based schemes, are also superior to the benchmark based on the center frequency. This also reveals the efficiency of the proposed scheme in face of the large-scale phenomenon and beam-squint effect. While the muti-user scenario exhibits similar tendencies to those in the single-user case, there are also some differences.

Fig. 10 (a) shows the achievable sum-rate versus the RIS scale N. Observe that when the scale is less then 240, the

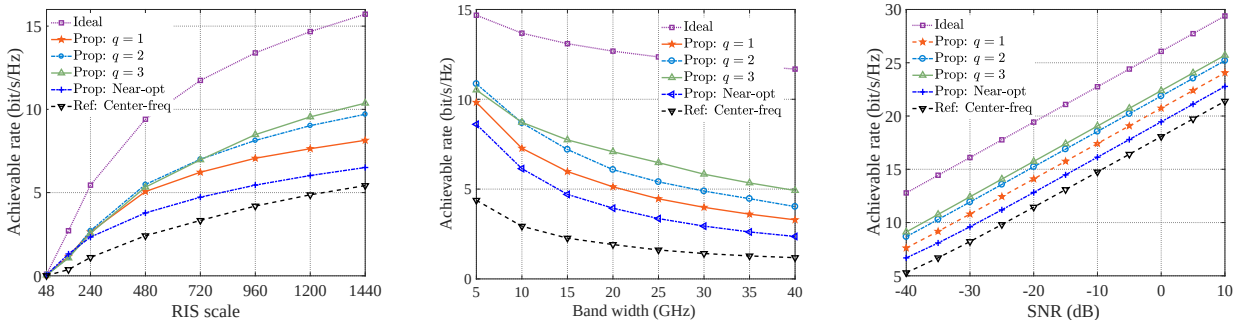

(a) Achievable rate v.s. RIS scale. (b) Achievable rate v.s. BW. (c) Achievable rate v.s. SNR.

Fig. 9. Achievable rate in single-user case.

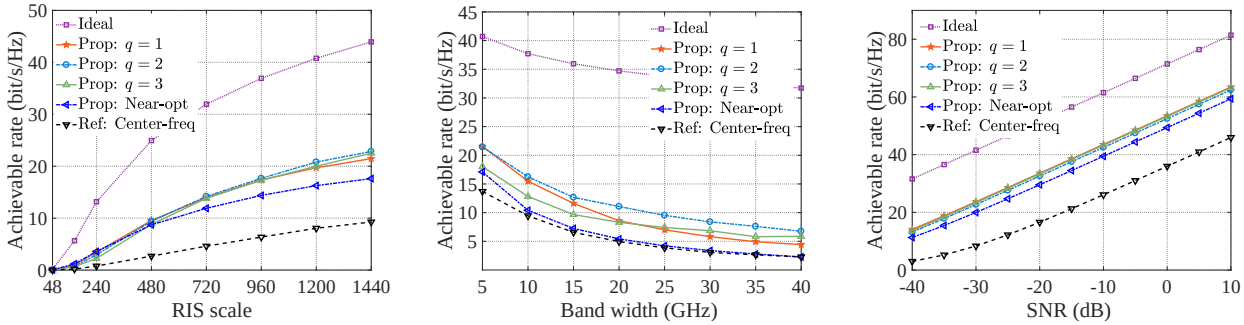

(a) Achievable rate v.s. RIS scale. (b) Achievable rate v.s. BW. (c) Achievable rate v.s. SNR.

Fig. 10. Achievable rate in muti-user case.

near-optimal scheme is the best option and the rates are at most the same for all the VSA-based shemes. The maximum rate is achieved for $q = 1$ and 2 when $240 < N < 480$ and $N > 480$. Compared to Fig. 9 (a), we find that for different numbers of users U, different q values should be chosen for rate maximization, because the array is virtually divided into U subarrays. This trend reveals even at a specifical scale, each subarray has reduced scale, a smaller q should be applied in the multi-user scenario. Moreover, the proposed VSA-based scheme achieves a 100% performance improvement in the multi-user case. For example, when $N = 1440$, for the proposed VSA-based scheme the sum-rate exceeds 20 bit/s/Hz, while it is less than 10 bit/s/Hz for the "Central" scheme.

Similarly, Fig. 10 (b) and Fig. 10 (c) present the achievable sum-rate for different BWs and SNRs, respectively. Furthermore, the proposed near-optimal scheme and the VSA-based scheme outperform the "Central" scheme. By jointly observing Fig. 9 (b) and Fig. 9 (c), we may find that the performance gain becomes smaller at a given scale, especially for a wider bandwidth. This is because the virtual partitioning of the array will result in a reduced-dimensional subarray allocated to an individual frequency, yielding a reduced array gain. On the other hand, for a wider bandwidth, the frequency dispersion becomes more severe owing to the aggravated beam-squint. Nevertheless, the VSA-based scheme can cope brightly with the beam concentration problem, which is not encountered in the single-user case. This will be detailed next

Fig. 11 illustrates the benefits of the proposed VSA-based scheme in avoiding the beam concentration issue. Specifically, Fig. 11 (a) depicts the achievable sum-rate of the near-optimal scheme where three cases are presented based on (37), corresponding to three random locations. As seen, for the near-optimal scheme, although the sum-rate can be improved compared to the "Central" scheme as seen in Fig. 10, the beam may be concentrated on an individual user, i.e., on user-1 in case-1, hence resulting in the performance erosion for the other users. The beam concentrates on user-2 and user-3 in case-2 and case-3 where the achievable rate of user-1 is degraded severely.

Fortunately, this problem can be avoided by the VSA-based scheme. Fig. 11 (b) shows the sum-rate of case-1 in Fig. 11 (a). It is clear that by leveraging the VSA-based scheme, not only the sum-rate is improved significantly, but also a beneficial performance balance among users has been achieved. This is an explicit benefit of the VSA division. On one hand, by partitioning the array into subarrays virtually according to the number of the users, multiple beams can be obtained, thereby enhancing the links between the RIS and all users, instead of only a single user or a fraction of the users. On the other hand, the beam-squint effect can be mitigated by the FDPS method at each subarray. Therefore, the VSA-based scheme not only mitigates the beam squint, but also avoids the beam concentration problem, thus improving the sum-rate.

Fig. 12 depicts the achievable sum-rate versus the number

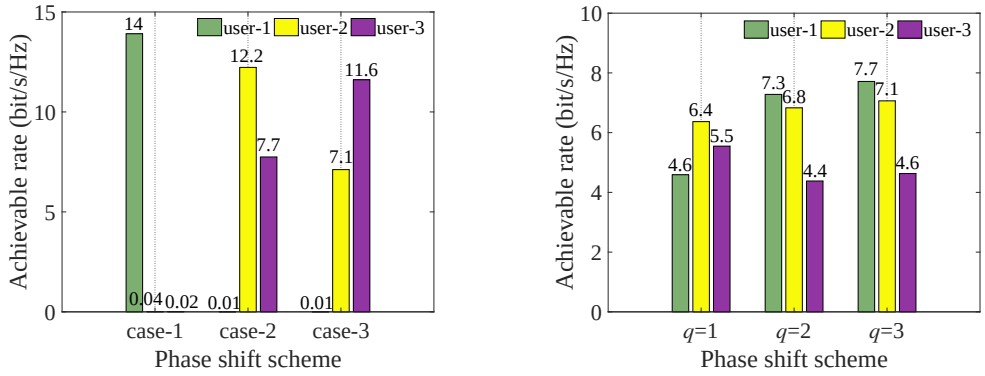

(a) Rate with near-optimal scheme.

(b) Rate with VSA-based scheme.

Fig. 11. Achievable rate with different phase design schemes.

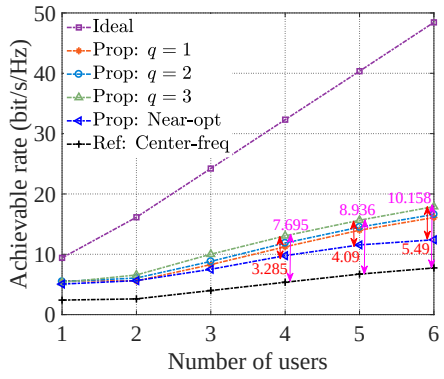

Fig. 12. Rate v.s. number of users.

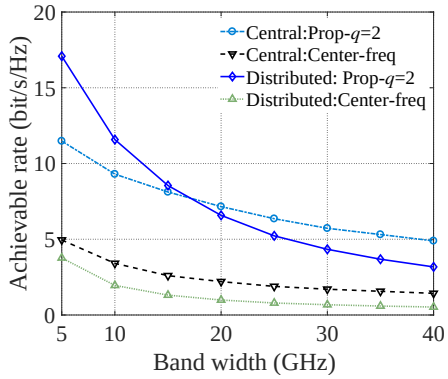

Fig. 13. Deployment comparison.

of users U. It is assumed that the number of RIS elements is 480, the distances between the users and the center of the RIS is 8 meters, and the angles between the users and RIS are independently and randomly distributed within $(0, 2\pi)$. As shown by Fig. 12, the proposed VSA-based scheme is superior to the reference scheme based on the central-frequency, and the advantage becomes more significant as the number of users increases. Take the results with $q = 3$ as an example, the performance gain of the VSA based scheme over the reference scheme is 7.695 bit/s/Hz with $U = 4$, and the gain increases to 10.158 bit/s/Hz for $U = 6$.

D. Discussion

According to the above discussions, we observe that the effectivity of dividing the RIS into multiple virtual sub-arrays, which indicates that the potential of distributed deployment. For example, Fig. 13 compares the centralized and distributed deployment of RIS in single-user case. Specifically, we adopt one RIS for the centralized deployment with $N = 1200$, and four RISs for the distributed deployment, each with the same size $N = 300$. As seen, with the phase shift based on center frequency, the performance of distributed deployment is not as good as that of centralized deployment. Additionally, for the distributed deployment, the performance with the proposed FDPS scheme with $q = 2$ surpasses that with center frequency. Last but not least, adopting the proposed FDPS scheme, the performance of distributed deployment outperforms that with centralized one when the bandwidth is relatively narrow. But, with the increase of bandwidth, the bean squint effect aggravates and the advantages of distributed deployment fade away. Nevertheless, the proposed FDPS scheme is superior to the phase shift design based on center frequency in both distributed and centralized deployments. Due to space limitations, the specific deployment strategies are not discussed in this paper.

VI. Conclusion

The achievable rate optimization of RIS-aided near-field wideband system was presented. Firstly, we analyzed the path loss of RIS-aided communication links, and provided the accurate manifold of the RIS in its near-field by taking both the large-scale phenomenon and the beam-squint effect into account. Based on the array manifold, we recast the achievable rate maximization problem and proposed phase design schemes for both single-uer and multi-user scenarios. Specifically, a near-optimal solution and the FDPS scheme were presented. We demonstrated that the latter effectively mitigate the beam squint effect in the single-user scenario. Moreover, a VSA-based scheme was proposed for mitigating the beam concentration problem involved in the multi-user

scenarios. Finally, numerical results validated the effectiveness of the proposed schemes in improving the achievable rate of near-field wideband communications. For instance, using the VSA-based phase design, the achievable sum-rate can be improved to more than twice when compared with the existing methods.

APPENDIX A

For easy of discussion, we assume that N is an odd values represented by $N = 2N' + 1$ with $N^{'}$ being an arbitrary integer. Naturally, the elements are labeled as $[-N^{'}, \ldots, 0, \ldots, N^{'}]$ with the 0^{th} representing the central element of the array. Additionally, d_0 and θ_0 denotes the distance and angle w.r.t. the 0^{th} element, respectively. According to the geometry, we have $d_n = \sqrt{d_0^2 + n^2 d_e^2 - 2nd_e d_0 \sin\theta_0}, n \in [-N^{'}, \ldots, 0, \ldots, N^{'}]$. By defining $\gamma = d_e/d_0$, we have

$$\begin{aligned} &\left|\mathbf{b}^*\left(N, \mathbf{d}, f_k\right)\mathbf{b}\left(N, \mathbf{d}, f_i\right)\right| \\ &= \frac{1}{N}\sum_{n=-N^{'}}^{N^{'}}\left(\frac{1}{1+\gamma^2 n^2 - 2n\gamma\sin\theta_0}\right)^2 e^{j\frac{4\pi(f_k-f_i)\left(d_{N,u}-d_{1,u}\right)}{c}}. \end{aligned} \tag{42}$$

An approximation of the second term of (42) is given in (43) at the bottom of this page where the inequality (a) is due to $ae^{j\theta_a} + be^{j\theta_b} \leq a+b$. Additionally, the approximation (b) is obtained by exploiting the concept of definite integrals [28, Eq. (17)] and by substituting $x = \gamma n$. Moreover, (c) follows by the integration of a proper rational fraction [44, Eq. (2.103.3)]. By further transformations borrowed from trigonometric algebra, (18) can be obtained.

APPENDIX B

For the MRC scheme, associated with $\mathbf{w}_k = \mathbf{h}_k / \left\|\mathbf{h}_k\right\|$, the $\mathcal{P}2$ can be recast as

$$\mathcal{P}2(1): \quad \overline{R}_k = \max_{\mathbf{W},\boldsymbol{\Theta}} \log_2\left(1 + \frac{p\left\|\mathbf{h}_k\right\|^2}{\sigma^2}\right),\ s.t.\ \left|\left[\boldsymbol{\Theta}\right]_{n,k}\right| = 1. \tag{44}$$

Furthermore, with the aid of (20) and (21), we have $\left\|\mathbf{h}_k\right\|^2 = MN\alpha_1^2\alpha_{RB}^2\chi_k$, and the problem $\mathcal{P}2(1)$ becomes equivalent to

$$\mathcal{P}2(2): \quad \boldsymbol{\Theta} = \arg\max\ \chi_k,\ s.t.\ \left|\psi_{n,k}\right| = 1, \tag{45}$$

where we have

$$\chi_k = \sum_{n=1}^{N} A_n \frac{d_1^2}{d_n^2} e^{j\left[\psi_{n,k} + 4\epsilon_e\pi\frac{f_k}{f_c}(n-1)\sin\varphi_{BR} - \frac{4\pi f_k(d_n - d_1)}{c}\right]}, \tag{46}$$

with d_n denoting the distance between the user and the n^{th} RIS element, and $\epsilon_e = d_e/\lambda_c$ denoting the wave-length normalized spacing between adjacent RIS elements. As readily seen, χ_k can be maximized with all the summation terms being in phase, namely, each term in the brackets equals to zero. Hence, the phase in (24) and achievable rate in (25) can be obtained.

APPENDIX C

According to Jensen's inequality, we have

$$\sum_{k=1}^{K}\log_2\left(1 + \frac{p\left|\mathbf{w}_k^*\mathbf{h}_k\right|^2}{\sigma^2}\right) \leq \log_2\left(1 + \sum_{k=1}^{K}\frac{p\left|\mathbf{w}_k^*\mathbf{h}_k\right|^2}{\sigma^2}\right). \tag{47}$$

By exploiting $\mathbf{w}_k = \mathbf{h}_k / \left\|\mathbf{h}_k\right\|$, problem $\mathcal{P}1$ becomes

$$\mathcal{P}1(1): \quad \max_{\boldsymbol{\Theta}} \sum_{k=1}^{K}\left\|\mathbf{h}_k\right\|^2,\ s.t.\ \left|\left[\boldsymbol{\Theta}\right]_{n,k}\right| = 1. \tag{48}$$

Furthermore, the objective function (OF) in (48) can be recast as

$$\max_{\boldsymbol{\Theta}}\ MN\alpha_1^2\alpha_{RB}^2\sum_{k=1}^{K}\chi_k. \tag{49}$$

According to (46), to obtain a near-optimal phase shift for each RIS element, the above maximization problem can be connected to the following minimization problem

$$\begin{aligned} \mathcal{P}1(2): \ \min_{\psi_n}\frac{1}{K}\sum_{k=1}^{K}\Bigg|&\psi_n + 4\epsilon_e\pi\frac{f_k}{f_c}(n-1)\sin\varphi_{RB} \\ &- \frac{4\pi f_k\left(d_n - d_1\right)}{c}\Bigg|, \\ s.t.\ &\left|\psi_n\right| = 1 \end{aligned} \tag{50}$$

By defining $J_{n,k} = 4\pi f_k\left(\frac{d_n - d_1}{c} - \frac{\epsilon_e(n-1)\sin\varphi_{RB}}{f_c}\right)$, the OF in (50) can be rewritten as

$$\min_{\psi_n}\sum_{k=1}^{K}\left|\psi_n - J_{n,k}\right|. \tag{51}$$

$$\begin{aligned} &\sum_{n=-N^{'}}^{N^{'}}\left(\frac{1}{1+\gamma^2n^2-2n\gamma\sin\theta_0}\right)^2 e^{j\frac{4\pi(f_k-f_i)\left(d_{N,u}-d_{1,u}\right)}{c}} \overset{(a)}{\leq} \sum_{n=-N^{'}}^{N^{'}}\left(\frac{1}{1+\gamma^2n^2-2n\gamma\sin\theta_0}\right)^2 \\ &\overset{(b)}{\approx} \int_{-\gamma N^{'}}^{\gamma N^{'}}\frac{1}{\left(1-2\sin\theta_0 x + x^2\right)^2}dx \overset{(c)}{=} \frac{1}{\gamma\cos^3\theta_0}\left[\frac{1}{2\cos\theta_0}\left(\arctan\frac{\gamma N^{'} - \cos\theta_0\tan\theta_0}{\cos\theta_0}\right.\right. \\ &\left.\left.+\arctan\frac{\gamma N^{'} + \cos\theta_0\tan\theta_0}{\cos\theta_0}\right) + \frac{\gamma N^{'}\left(1 - 2\sin^2\theta_0 + \gamma^2 N^{'2}\right)}{\left(1+\gamma^2N^{'2}\right)^2 - 4\sin^2\theta_0\gamma^2N^{'2}}\right] \end{aligned} \tag{43}$$

Please note that $J_{n,1} \leq J_{n,2} \leq \cdots \leq J_{n,K}$, since $f_1 < f_2 < \cdots < f_K$.

Furthermore, we have

$$\begin{aligned}\sum_{k=1}^{K} |\psi_n - J_{n,k}| &= (|\psi_n - J_{n,1}| + |\psi_n - J_{n,K}|) \\ &\quad + (|\psi_n - J_{n,2}| + |\psi_n - J_{n,K-1}|) + \ldots' \\ &\overset{(a)}{\leq} |J_{n,1} - J_{n,K}| + |J_{n,2} - J_{n,K-1}| + \ldots\end{aligned} \tag{52}$$

where the process (a) follows by exploiting $|x-a|+|x-b| \leq |a-b|$. Additionally, the equation only holds, when ψ_n is between $J_{n,1}$ and $J_{n,K}$, and between $J_{n,2}$ and $J_{n,K-1}$, and so on. Hence, we have the following conclusion:

$$\psi_n = \begin{cases} \frac{J_{n,K/2}+J_{n,K/2+1}}{2}, \text{ when } \mod(K,2) = 0 \\ J_{n,(K+1)/2}, \text{ when K } \mod(K,2) = 1 \end{cases}; \tag{53}$$

upon substituting $f_k = f_c + \frac{B}{K}\left(k - \frac{K+1}{2}\right)$ into (53), (26) can be obtained. Then the proof ends.

APPENDIX D

Upon using MRC beamforming at the BS, the total achievable rate of U users over the whole band is given by

$$\begin{aligned} R_{\text{MU}} &= \frac{1}{K}\sum_{u=1}^{U}\sum_{k=1}^{K} \log_2\left(1 + \frac{p\left\|\mathbf{h}_{u,k}\right\|^2}{p\sum_{i=1,i\neq u}^{U}\frac{\left|\mathbf{h}_{u,k}^{*}\mathbf{h}_{i,k}\right|^2}{\left\|\mathbf{h}_{u,k}\right\|^2} + \sigma^2}\right) \\ &\leq \frac{1}{K}\sum_{u=1}^{U}\sum_{k=1}^{K} \log_2\left(1 + \frac{p\left\|\mathbf{h}_{u,k}\right\|^2}{\sigma^2}\right) \\ &\overset{(a)}{\leq} \log_2\left(1 + \frac{p}{\sigma^2}\frac{1}{K}\sum_{u=1}^{U}\sum_{k=1}^{K}\left\|\mathbf{h}_{u,k}\right\|^2\right) \\ &\overset{(b)}{=} \log_2\left(1 + \frac{p\alpha_{RB}MN^2}{\sigma^2}\frac{1}{K}\sum_{u=1}^{U}\sum_{k=1}^{K}\alpha_u\left|\chi_{u,k}\right|^2\right) \end{aligned}, \tag{54}$$

where the process (a) followes by exploiting Jensen's inequality and (b) is due to $\left\|\mathbf{a}\left(M,\theta_{RB},f_k\right)\right\|^2 = 1$. Additionally,

$$\begin{aligned}\chi_{u,k} &= \mathbf{a}^{*}\left(N,\varphi_{RB},f_k\right)\boldsymbol{\Theta}\mathbf{b}\left(N,\mathbf{d}_u,f_k\right) \\ &= \sum_{n=1}^{N}\frac{d_{1,u}^2}{d_{n,u}^2}e^{j\left[\psi_n + 4\epsilon_e\pi\frac{f_k}{f_c}(n-1)\sin\varphi_{BR} - \frac{4\pi f_k\left(d_{n,u}-d_{1,u}\right)}{c}\right]}.\end{aligned} \tag{55}$$

Naturally, the near-optimal problem of $\mathcal{P}3$ is given by

$$\mathcal{P}3(1):\ \min\ \sum_{u=1}^{U}\sum_{k=1}^{K}\left|\psi_n - J_{n,u,k}\right|, \tag{56}$$

with $J_{n,u,k} = 4\pi f_k[\left(d_{n,u} - d_{1,u}\right)/c - \epsilon_e\left(n-1\right)\sin\varphi_{RB}/f_c]$. Please note that $J_{n,u,1} \leq J_{n,u,2} \leq \cdots \leq J_{n,u,K}$ for $u \in \{1,2,\ldots,U\}$ and $n \in \{1,2,\ldots,N\}$. Similar to the process of (51)-(53), we obtain the optimal phase shift in (37) for multiple users scenarios. Then, the proof ends.

REFERENCES

[1] B. Yang *et al.*, "Spectrum learning-aided reconfigurable intelligent surfaces for 'green' 6G networks", *IEEE Network*, vol. 35, no. 6, pp. 20-26, Nov. 2021.

[2] M. D. Renzo *et al.*, "Smart radio environments empowered by AI reconfigurable meta-surfaces: An idea whose time has come", *EURASIP J. Wireless Commun. Netw.*, vol. 2019, no. 1, pp. 1-20, May 2019.

[3] C. Huang *et al.*, "Reconfigurable intelligent surfaces for energy efficiency in wireless communication," *IEEE Trans. Wireless Commun.*, vol. 18, no. 8, pp. 4157-4170, Aug. 2019.

[4] C. Pradhan *et al.*, "Hybrid precoding design for reconfigurable intelligent surface aided mmWave communication systems," *IEEE Wireless Commun. Lett.*, vol. 9, no. 7, pp. 1041-1045, Jul. 2020.

[5] P. Wang *et al.*, "Intelligent reflecting surface-assisted millimeter wave communications: Joint active and passive precoding design," *IEEE Trans. Veh. Technol.*, vol. 69, no. 12, pp. 14960-14973, Dec. 2020.

[6] W. Chen *et al.*, "Sum-rate maximization for intelligent reflecting surface based Terahertz communication systems," in *Proc. IEEE/CIC Int. Conf. Commun. Workshops China*, Changchun, China, 2019, pp. 153-157.

[7] Q. Wu *et al.*, "Energy efficient intelligent reflecting surface assisted Terahertz communications," in *Proc. IEEE Int. Conf. Commun. Workshops*, Montreal, QC, Canada, 2021, pp. 1-6.

[8] C. Huang *et al.*, "Multi-hop RIS-empowered terahertz communications: A DRL-based hybrid beamforming design," *IEEE J. Sel. Areas Commun.*, vol. 39, no. 6, pp. 1663-1677, Jun. 2021.

[9] B. Ning *et al.*, "Terahertz multi-user massive MIMO with intelligent reflecting surface: Beam training and hybrid beamforming," *IEEE Trans. Veh. Technol.*, vol. 70, no. 2, pp. 1376-1393, Feb. 2021.

[10] Y. Cheng and W. Peng, "Codebook-based phase adjustment for IRS-aided communication via time-coding modulation," in *Proc. IEEE Int. Global Commun. Conf.*, Taipei, Taiwan, 2020, pp. 1-6.

[11] S. Abeywickrama, R. Zhang, Q. Wu and C. Yuen, "Intelligent reflecting surface: Practical phase shift model and beamforming optimization," *IEEE Trans. Commun.*, vol. 68, no. 9, pp. 5849-5863, Sept. 2020.

[12] E. Björnson and L. Sanguinetti, "Power scaling laws and near-field behaviors of massive MIMO and intelligent reflecting surfaces," *IEEE Open J. Commun. Society*, vol. 1, pp. 1306-1324, 2020.

[13] F. H. Danufane *et al.*, "On the path-loss of reconfigurable intelligent surfaces: An approach based on Green's theorem applied to vector fields," *IEEE Trans. Commun.*, vol. 69, no. 8, pp. 5573-5592, Aug. 2021.

[14] Ö. Özdogan, E. Björnson and E. G. Larsson, "Intelligent reflecting surfaces: Physics, propagation, and pathloss modeling," *IEEE Wireless Commun. Lett.*, vol. 9, no. 5, pp. 581-585, May 2020.

[15] M. Najafi, V. Jamali, R. Schober and H. V. Poor, "Physics-based modeling and scalable optimization of large intelligent reflecting surfaces," *IEEE Trans. Commun.*, vol. 69, no. 4, pp. 2673-2691, Apr. 2021.

[16] Y. Cheng *et al.*, "RIS-aided wireless communications: Extra degrees of freedom via rotation and location optimization," *IEEE Trans. Wireless Commun.*. Early Access. doi: 10.1109/TWC.2022.3151702

[17] W. Tang *et al.*, "Wireless communications with reconfigurable intelligent surface: Path loss modeling and experimental measurement," *IEEE Trans. Wireless Commun.*, vol. 20, no. 1, pp. 421-439, Jan. 2021.

[18] H. Sarieddeen, M.-S. Alouini and T. Y. Al-Naffouri, "An overview of signal processing techniques for Terahertz communications," *Proc. IEEE*, vol. 109, no. 10, pp. 1628-1665, Oct. 2021.

[19] B. Wang, F. Gao, S. Jin, H. Lin and G. Y. Li, "Spatial and frequency-wideband effects in millimeter-wave massive MIMO systems," *IEEE Trans. Signal Process.*, vol. 66, no. 13, pp. 3393-3406, Jul. 2018.

[20] Y. Chen, Y. Xiong, D. Chen, T. Jiang, S. X. Ng and L. Hanzo, "Hybrid precoding for wideband millimeter wave MIMO systems in the face of beam squint," *IEEE Trans. Wireless Commun.*, vol. 20, no. 3, pp. 1847-1860, Mar. 2021.

[21] R. Zhang, W. Hao, G. Sun, and S. Yang, "Hybrid precoding design for wideband THz massive MIMO-OFDM systems with beam squint," *IEEE Syst. J.*, vol. 15, no. 3, pp. 3925-3928, Sep. 2021.

[22] L. Dai, J. Tan, Z. Chen, and H. V. Poor, "Delay-phase precoding for wideband THz massive MIMO," *IEEE Trans. Wireless Commun.*, vol. 21, no. 9, pp. 7271-7286, Sept. 2022.

[23] Y. Chen *et al.*, "Beam-squint mitigating in reconfigurable intelligent surface aided wideband mmWave communications," in *Proc. IEEE Wireless Commun. Netw. Conf.*, Nanjing, China, 2021, pp. 1-6.

[24] W. Hao, X. You, F. Zhou, Z. Chu, G. Sun and P. Xiao, "The Far-/Near-Field Beam Squint and Solutions for THz Intelligent Reflecting Surface Communications," *IEEE Trans. Veh. Technol.*

[25] P. Yang *et al.*, "6G wireless communications: Vision and potential techniques," *IEEE Net.*, vol. 33, no. 4, pp. 70-75, Jul./Aug. 2019.

[26] C. Huang *et al.*, "Holographic MIMO surfaces for 6G wireless networks: Opportunities, challenges, and trends", *IEEE Wireless Commun.*, vol. 27, no. 5, pp. 118-125, Oct. 2020.

[27] M. Cui, L. Dai, R. Schober, L. Hanzo, "Near-field wideband beamforming for extremely large antenna array," Sept. 2021, arXiv:2109.10054. [Online]. Available: http://arxiv.org/abs/2109.10054

[28] H. Lu and Y. Zeng, "How does performance scale with antenna number for extremely large-scale MIMO?" *in Proc. IEEE Int. Conf. Commun.*, 2021, pp. 1-6.

[29] J. Jiang and M. A. Ingram, "Spherical-wave model for short-range MIMO," *IEEE Trans. Commun.* , vol. 53, no. 9, pp. 1534-1541, Sept. 2005.

[30] N. Decarli, D. Dardari, "Communication modes with large intelligent surfaces in the near field," *IEEE Access*, vol. 9, pp. 165648-165666, 2021.

[31] C. A. Balanis, Antenna Theory: Analysis and Design, 4th ed. New York: Wiley, 2016.

[32] M. Cui, L. Dai, "Channel estimation for extremely large-scale MIMO: Far-field or near-Field?" *IEEE Trans. Commun.*, vol. 70, no. 4, pp. 2663-2677, April 2022.

[33] K. Dovelos *et al.*, "Electromagnetic modeling of holographic intelligent reflecting surfaces at Terahertz bands," Aug. 2021, arXiv:2108.08104. [Online]. Available: http://arxiv.org/abs/2108.08104.

[34] M. A. Eimossallamy *et al.*, "Reconfigurable intelligent surfaces for wireless communications: Principles, challenges, and opportunities," *IEEE Trans. Cogn. Commun. Net.*, vol. 6, no. 3, pp. 990-1002, Sept. 2020.

[35] K. Rouhi, S. E. Hosseininejad, S. Abadal, M. Khalily and R. Tafazolli, "Multi-Channel Near-Field Terahertz Communications Using Reprogrammable Graphene-Based Digital Metasurface," *J. Lightwave Technol.*, vol. 39, no. 21, pp. 6893-6907, 1 Nov.1, 2021.

[36] K. Liu, Z. Zhang, L. Dai and L. Hanzo, "Compact user-specific reconfigurable intelligent surfaces for uplink transmission," *IEEE Trans. Commun.*, vol. 70, no. 1, pp. 680-692, Jan. 2022.

[37] B. Wang *et al.*, "Spatial-wideband effect in massive MIMO with application in mmWave systems," *IEEE Commun. Mag.*, vol. 56, no. 12, pp. 134-141, Dec. 2018.

[38] B. Ning *et al.*, "Prospective beamforming technologies for ultra-massive MIMO in terahertz communications: A tutorial," Jul. 2021, arXiv:2107.03032. [Online]. Available: http://arxiv.org/abs/2107.03032

[39] B. Friedlander, "Localization of signals in the near-field of an antenna array," *IEEE Trans. Signal Process.*, vol. 67, no. 15, pp. 3885-3893, 1 Aug.1, 2019.

[40] K. Zhi *et al.*, "Reconfigurable intelligent surface-aided MISO systems with statistical CSI: Channel estimation, analysis and optimization," in *Proc. IEEE 22nd Int. Workshop Signal Process. Adv. Wireless Commun.*, Lucca, Italy, 2021, pp. 576-580.

[41] L. Wei *et al.*, "Channel estimation for RIS-empowered multi-user MISO wireless communications," *IEEE Trans. Commun.*, vol. 69, no. 6, pp. 4144-4157, Jun. 2021.

[42] B. Di, H. Zhang, L. Song, Y. Li, Z. Han and H. V. Poor, "Hybrid beamforming for reconfigurable intelligent surface based multi-user communications: Achievable rates with limited discrete phase shifts," *IEEE J. Sel. Areas Commun.*, vol. 38, no. 8, pp. 1809-1822, Aug. 2020.

[43] H. Q. Ngo *et al.*, "Energy and spectral efficiency of very large multiuser MIMO systems," *IEEE Trans. Commun.*, vol. 61, no. 4, pp. 1436-1449, Apr. 2013.

[44] I. S. Gradshteyn and I. M. Ryzhik, Table of Integrals, Series, and Products, 7th ed. San Diego, CA, USA: Academic, 2000, pp. 67-70.

[45] K. A. Alnajjar, P. J. Smith, G. K. Woodward and D. A. Basnayaka, "Design and analysis of a reduced complexity MRC V-BLAST receiver for massive MIMO," in *Proc. 2016 IEEE 17th Inter. Workshop Signal Process. Advances Wireless Commun*, Edinburgh, UK, 2016, pp. 1-5.

[46] C. Siriteanu and S. D. Blostein, "Maximal-ratio eigen-combining for smarter antenna arrays," *IEEE Trans. Wireless Commun.*, vol. 6, no. 3, pp. 917 C 925, March 2007.

Yajun Cheng received his B.Sc. and the M.Sc. degrees from Chongqing University of Posts and Telecommunications, Chongqing, China, in 2015 and 2018, respectively, and his PhD degree from Huazhong University of Science and Technology, Wuhan, China, in 2022. In 2021 and 2022, he was a Visiting Student with the School of Electrical and Electronics Engineering, Nanyang Technological University, and the Engineering Product Development Pillar, Singapore University of Technology and Design, Singapore. His research interests include reconfigurable intelligent surfaces, signal processing for wireless communications.

Chongwen Huang (Member, IEEE) obtained his B. Sc. degree in 2010 from Nankai University, and the M.Sc degree from the University of Electronic Science and Technology of China in 2013, and PhD degree from Singapore University of Technology and Design (SUTD) in 2019. From Oct. 2019 to Sep. 2020, he is a Postdoc in SUTD. Since Sep. 2020, he joined into Zhejiang University as a tenure-track young professor. Dr. Huang is the recipient of 2021 IEEE Marconi Prize Paper Award, 2023 IEEE Fred W. Ellersick Prize Paper Award and 2021 IEEE ComSoc Asia-Pacific Outstanding Young Researcher Award. He has served as an Editor of IEEE Communications Letter, Elsevier Signal Processing, EURASIP Journal on Wireless Communications and Networking and Physical Communication since 2021. His main research interests are focused on Holographic MIMO Surface/Reconfigurable Intelligent Surface, B5G/6G Wireless Communications, mmWave/THz Communications, Deep Learning technologies for Wireless communications, etc.

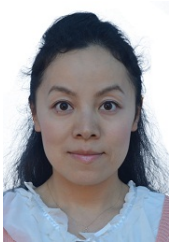

Wei Peng (M07-SM12) received the Ph.D. degree in wireless communications from the University of Hong Kong, Hong Kong, in 2007. She was a Postdoctoral Research Fellow from 2008 to 2009 and an Assistant Professor from 2009 to 2013 with Tohoku University, Sendai, Japan. Since 2013, she has been an Professor with the School of Cyber Science and Engineering, Huazhong University of Science and Technology, and Research Center of 6G Mobile Communications, Wuhan, China. She held a visiting position with Columbia University, New York, NY, USA. Her research interests include signal processing for large-scale wireless communication systems, online learning based network optimization, and space-ground integrated networks.

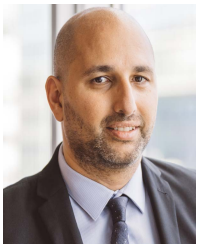

Mérouane Debbah (Fellow, IEEE) is a researcher, educator and technology entrepreneur. Over his career, he has founded several public and industrial research centers, start-ups and is now a Professor at Khalifa University of Science and Technology in Abu Dhabi and founding Director of the 6G center. He is a frequent keynote speaker at international events in the field of telecommunication and AI. His research has been lying at the interface of fundamental mathematics, algorithms, statistics, information and communication sciences with a special focus on random matrix theory and learning algorithms. In the Communication field, he has been at the heart of the development of small cells (4G), Massive MIMO (5G) and Large Intelligent Surfaces (6G) technologies. In the AI field, he is known for his work on Large Language Models, distributed AI systems for networks and semantic communications. He received multiple prestigious distinctions, prizes and best paper awards (more than 35 best paper awards) for his contributions to both fields and according to research.com is ranked as the best scientist in France in the field of Electronics and Electrical Engineering. He is an IEEE Fellow, a WWRF Fellow, a Eurasip Fellow, an AAIA Fellow, an Institut Louis Bachelier Fellow and a Membre émérite SEE.

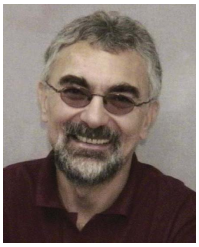

Lajos Hanzo (Life Fellow, IEEE) received the masters and Ph.D. degrees from the Technical University (TU) of Budapest in 1976 and 1983, respectively, the Doctor of Sciences (D.Sc.) degree from the University of Southampton in 2004, the Honorary Doctorate from the TU of Budapest in 2009, and the Honorary Doctorate from the University of Edinburgh in 2015. He is a Foreign Member of the Hungarian Science-Academy, Fellow of the Royal Academy of Engineering (FREng), of the IET, of EURASIP and holds the IEEE Eric Sumner Technical Field Award. (http://www-mobile.ecs.soton.ac.uk/; https://en.wikipedia.org/wiki/Lajos_Hanzo)

Chau Yuen (S02-M06-SM12-F21) received the B.Eng. and Ph.D. degrees from Nanyang Technological University, Singapore, in 2000 and 2004, respectively. He was a Post-Doctoral Fellow with Lucent Technologies Bell Labs, Murray Hill, in 2005, and a Visiting Assistant Professor with The Hong Kong Polytechnic University in 2008. From 2006 to 2010, he was with the Institute for Infocomm Research, Singapore. From 2010 to 2023, he was with the Engineering Product Development Pillar, Singapore University of Technology and Design. Since 2023, he has been with the School of Electrical and Electronic Engineering, Nanyang Technological University.

Dr. Yuen received IEEE ICC Best Paper Award (2023), IEEE Communications Society Fred W. Ellersick Prize (2023), IEEE Marconi Prize Paper Award in Wireless Communications (2021), and EURASIP Best Paper Award for JOURNAL ON WIRELESS COMMUNICATIONS AND NETWORKING (2021). He was a recipient of the Lee Kuan Yew Gold Medal, the Institution of Electrical Engineers Book Prize, the Institute of Engineering of Singapore Gold Medal, the Merck Sharp and Dohme Gold Medal, and twice a recipient of the Hewlett Packard Prize. He received the IEEE Asia Pacific Outstanding Young Researcher Award in 2012 and IEEE VTS Singapore Chapter Outstanding Service Award on 2019.

Dr. Yuen current serves as an Editor-in-Chief for Springer Nature Computer Science, Editor for IEEE TRANSACTIONS ON VEHICULAR TECHNOLOGY, IEEE SYSTEM JOURNAL, and IEEE TRANSACTIONS ON NETWORK SCIENCE AND ENGINEERING, where he was awarded as IEEE TNSE Excellent Editor Award and Top Associate Editor for TVT from 2009 to 2015. He also served as the guest editor for several special issues, including IEEE JOURNAL ON SELECTED AREAS IN COMMUNICATIONS, IEEE WIRELESS COMMUNICATIONS MAGAZINE, IEEE COMMUNICATIONS MAGAZINE, IEEE VEHICULAR TECHNOLOGY MAGAZINE, IEEE TRANSACTIONS ON COGNITIVE COMMUNICATIONS AND NETWORKING, and ELSEVIER APPLIED ENERGY.

He is a Distinguished Lecturer of IEEE Vehicular Technology Society, Top 2% Scientists by Stanford University, and also a Highly Cited Researcher by Clarivate Web of Science. He has 3 US patents and published over 500 research papers at international journals or conferences.